JOURNAL OF PROPULSION AND POWER
Vol. 18, No. 3, May–June 2002

High-Pressure Steam Flow in Turbine Bypass Valve System Part 1: Valve Flow

R. S. Amano* and G. R. Draxler†
University of Wisconsin—Milwaukee, Milwaukee, Wisconsin 53201

This paper presents a study of steam flow behavior through a high-pressure turbine bypass valve when it suffers a high-pressure reduction in an electric-power-plant cogenerator system. Efforts have been mainly directed at investigating the process of steam flow and property variations in the aforementioned bypass valve as well as at obtaining correlations between the flow rate and the valve opening ratio. Modeling of the high-pressure turbulent steam flow was performed on a three-dimensional nonstaggered grid system by employing the finite volume differencing method and by solving the three-dimensional, turbulent, compressible Navier–Stokes and energy equations. Through this research numerous data have been acquired and analyzed. These efforts enable us to obtain a correlation data set for the valve-opening vs the flow rate coefficient of the valve. One of the significant accomplishments is to use the model presented here to further improve the design of a high-pressure steam turbine bypass flow valve to reduce a high-velocity spot in the valve flow pass so that noise can be suppressed.

Nomenclature

C_g	=	gas sizing coefficient
C_l	=	constant used in the near-wall model
$C_{\varepsilon 1}$, $C_{\varepsilon 2}$	=	constants used in the source terms of the turbulence energy dissipation
C_μ	=	constant used in calculation of turbulent eddy viscosity
c_p	=	specific heat for constant pressure
f_k	=	coriolis force
f_μ	=	damping function
h	=	enthalpy
h'	=	turbulent enthalpy fluctuation
J	=	Jacobian metric
K	=	coefficient of porous plate
k	=	turbulence kinetic energy
P	=	mean pressure
P_k	=	generation rate of turbulent kinetic energy
$\dot{q}$	=	heat-transfer rate
$\dot{q}$	=	heat flux per unit area
$\dot{q}_w$	=	wall heat flux per unit area
r, θ, z	=	polar cylindrical coordinates
R_t	=	turbulence Reynolds number
T	=	mean temperature
U	=	streamwise velocity component
u	=	fluctuating velocity in x direction
$\overline{u_i u_j}$	=	Reynolds stresses
V	=	mean velocity in radial direction
W	=	mean velocity in azimuth direction
y	=	coordinate normal to wall
y^+	=	dimensionless distance
α	=	thermal diffusivity
β	=	permeability of porosity
γ_T	=	spatial deviations from T
γ_U	=	spatial deviations from U
δ_{ij}	=	Kronecker delta
ε	=	turbulence energy dissipation rate
ε_{ij}	=	dissipation rate of $\overline{u_i u_j}$
κ	=	von Kármán constant
λ	=	thermal conductivity
μ	=	dynamic viscosity
μ_{eff}	=	effective viscosity, $\mu + \mu_t$
μ_t	=	turbulent dynamic viscosity
ν	=	kinematic viscosity, μ/ρ
ν_{eff}	=	effective kinematic viscosity, $\nu + \nu_t$
ν_t	=	kinematic eddy viscosity
ξ, η, ζ	=	curvilinear coordinates
ρ	=	density of fluid
σ_k	=	turbulent Prandtl number for k
σ_ε	=	turbulent Prandtl number for $\gamma = \kappa C_\mu^{-\frac{1}{2}}/(C_{\varepsilon 2} - C_{\varepsilon 1})$
$\langle\ \rangle$	=	volume-averaged values

Subscripts

i, j, k, l	=	tensor notations in inlet station conditions
in	=	inlet station conditions
w	=	wall values

Introduction

THE high-pressure and high-temperature turbine bypass valve is used in steam turbines of the cogenerator system of a power plant to control the flow rate through a steam turbine. Some of the problems occurring in many power plants are 1) noise problem caused by a high-speed flow in the valve where about 100 atm of pressure is required to be reduced down to 5 ~ 7 atm and 2) a high pressure that frequently causes cracking in the components caused by fatigue, etc. Therefore, a technique is needed to quickly investigate flow performance in a valve for prevention of noise and failure and for improvements of the designs. Efforts have been mainly directed at investigating the process of steam flow and property variations through the high-pressure turbine bypass valve so that a correlation between the flow rate and the valve-openingratio can be obtained. This can, thus, be utilized for the future improvement of such valve systems.

This paper presents a study on the mechanisms for controlling steam temperature in a bypass pipe system. The analysis has been performed by using a numerical method to review the system to enhance the efficiency and life of the units. For the simulations of steam flow behavior through a very complex geometry, both turbulence and numerical studies are crucial for proper evaluations of the heat transfer and evaporation processes. Numerous turbulence

Received 4 March 1999; revision received 10 August 2001; accepted for publication 22 August 2001.

*Professor, Department of Mechanical Engineering, EMS Building.
†Research Assistant, Department of Mechanical Engineering.

models using a higher-order closure model have been reported.[1–4] Numerical models using the body-fitted boundary coordinates were developed by many researchers,[5–8] and these models were applied to numerous internal flowpath problems as well as external flows. Maruszewski and Amano[9] and Amano and He[10] demonstrated that an adaptive grid-generation technique is particularly advantageous for computations of a flow that is bounded by solid boundaries with a complex geometry.

To conduct the tasks just mentioned, computational methods were employed using a finite volume method. Modeling of the high-pressure turbulent steam flow was successfully accomplished using three-dimensional, turbulent, compressible flow, and heat-transfer formulations. The governing equations were discretized on a curvilinear grid to enable computations in an irregular geometry. A nonstaggered grid system is used for discrete velocities and pressures. Interpolation was accomplished via a higher-order numerical scheme.

Turbulent flows were solved by employing a nonlinear version of the k–ε model. Here the computations performed show very encouraging results when compared with experimental data and theoretical results.

Problem Specifications

The model of the high-pressure steam bypass valve is shown in Fig. 1 (units are in millimeters). The head of the valve is illustrated in Fig. 1b. Steam at 122 atm enters the valve through a 189.4-mm-diam port (shown at the exit boundary on right-hand side of the figure in Fig. 1a, and then the flow is directed to the pipeline connecting to the condenser. As shown in this figure, a half of the entire valve is modeled because of its symmetric configuration. The model also includes the upper portion of the pipe downstream of the valve (approximately two diameters of the pipe length). In this way the flow in the pipe can be investigated. The pressure drop is forced through a perforated bell-shaped container called a "whisper cage," which is illustrated in Fig. 1c. As is mentioned later, this whisper cage was modeled by using a computational technique of the flow-through porous media.

Mathematical Models

Governing Equations

For the steady-state turbulent flows the averaged governing equations are given as follows:

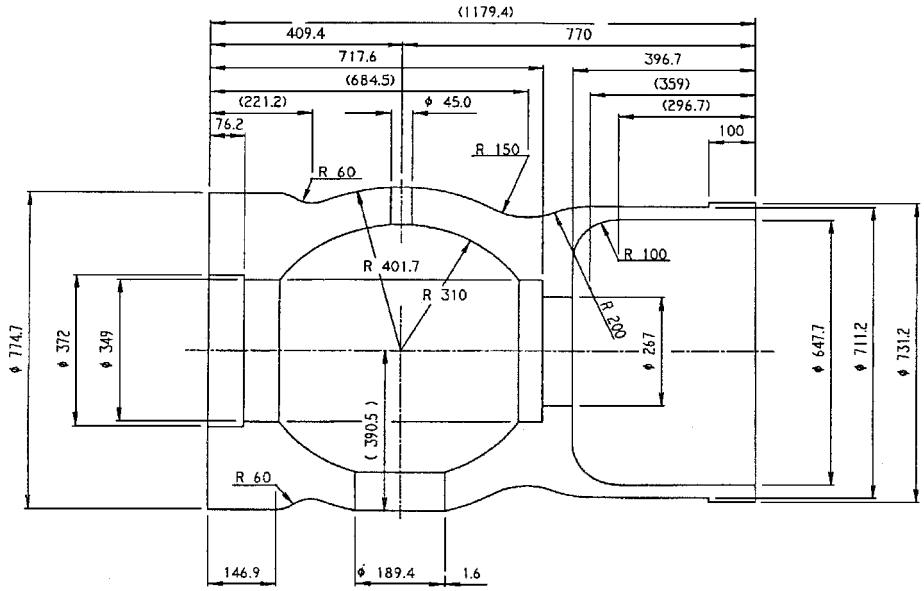

a) Valve cross section

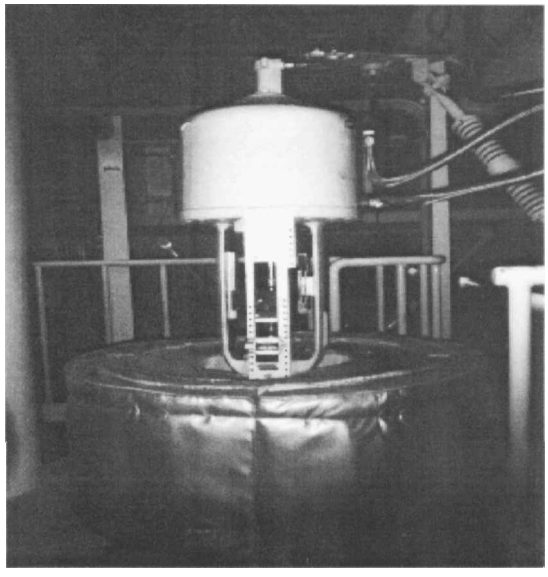

b) Valve head

c) Whisper cage

Fig. 1 Steam turbine bypass valve.

Continuity:

$$\frac{\partial \rho U_i}{\partial x_i} = 0 \tag{1}$$

Momentum:

$$\rho\left(\frac{\partial U_i U_j}{\partial x_j} + \varepsilon_{ikj} U_j f_k\right) = -\frac{\partial P}{\partial x_i} + \frac{\partial}{\partial x_j}\left(\mu \frac{\partial U_i}{\partial x_j} - \overline{\rho u_i u_j}\right) \tag{2}$$

These stresses ($-\overline{u_i u_j}$) can be determined from the Boussinesq assumption in which the Reynolds stresses are linearly related with strain tensors, that is,

$$-\overline{\rho u_i u_j} = -\frac{2}{3}\delta_{ij} + \mu_t\left(\frac{\partial U_i}{\partial x_j} + \frac{\partial U_j}{\partial x_i}\right) \tag{3}$$

Energy:

$$\rho \frac{\partial h U_j}{\partial x_j} = \frac{\partial}{\partial x_j}\left(\frac{\partial h}{\partial x_j} - \overline{\rho h' u_j}\right) \tag{4}$$

Turbulence Model

In the standard k–ε model the turbulence dynamic viscosity is given by

$$\mu_t = C_\mu(\rho k^2/\varepsilon) \tag{5}$$

Both the turbulence kinetic energy and the turbulence energy dissipation rate are determined from their own transport equations of the forms shown as follows:

Turbulence kinetic energy:

$$\rho U_i \frac{\partial k}{\partial x_i} = \frac{\partial}{\partial x_i}\left[\left(u + \frac{u_t}{\sigma_k}\right)\frac{\partial k}{\partial x_i}\right] - \rho(P_k - \varepsilon) \tag{6}$$

Turbulence energy dissipation rate:

$$\rho U_i \frac{\partial \varepsilon}{\partial x_i} = \frac{\partial}{\partial x_i}\left[\left(\mu + \frac{\mu_t}{\sigma_\varepsilon}\right)\frac{\partial \varepsilon}{\partial x_i}\right] - \frac{\rho\varepsilon}{k}(C_{\varepsilon 1} P_k - C_{\varepsilon 2}\varepsilon) \tag{7}$$

where

$$P_k = -\overline{u_i u_j}\frac{\partial U_i}{\partial x_j} \tag{8}$$

In the near-wall region the high-Reynolds-number version of the preceding equations does not simulate correctly. Therefore, the one-equation model of turbulence by Iacovides and Launder[11] was employed. In this model the dissipation rate and turbulence viscosity near the wall are calculated with the prescribed length scale l_μ and l_ε, that is;

$$\mu_t = C_\mu \rho \sqrt{k} l_\mu \tag{9}$$

where

$$\varepsilon = k^{\frac{3}{2}} / l_\varepsilon \tag{10}$$

and

$$l_\varepsilon = \left(\kappa \Big/ C_\mu^{\frac{3}{4}}\right) y[1 - \exp(-0.263 y^+)] \tag{11}$$

where y^+ is defined as

$$y^+ = y\left(\sqrt{k}/\nu\right) \tag{12}$$

In the preceding equations C, $C_{\varepsilon 1}$, $C_{\varepsilon 2}$, κ are constants whose values are 0.09, 1.45, 1.92, and 0.42, respectively.

For the improvement of the low-Reynolds-number effect, Launder–Sharma model[12] (L–S) turbulence viscosity is damped in the near-wall region. Thus,

$$\mu_t = C_\mu f_\mu \rho(k^2/\tilde{\varepsilon}) \tag{13}$$

where f is calculated from the following equation:

$$f_\mu = \exp\left[\frac{-3.4}{(1 + 0.02R_t)^2}\right] \tag{14}$$

where R_t is given as

$$R_t = k^2/\mu\tilde{\varepsilon} \tag{15}$$

where $\tilde{\varepsilon}$ is defined as

$$\tilde{\varepsilon} = \varepsilon - 2\mu\left(\frac{\partial k^{\frac{1}{2}}}{\partial x_j}\right)^2 \tag{16}$$

The kinetic-energy equation is the same as Eq. (6). However, the dissipation-rate equation has a different form from Eq. (7), which is given as

$$\rho U_i \frac{\partial \tilde{\varepsilon}}{\partial x_i} = \frac{\partial}{\partial x_i}\left[\left(\mu + \frac{\mu_t}{\sigma_\varepsilon}\right)\right] - \rho\frac{\tilde{\varepsilon}}{k}(C_{\varepsilon 1} f_{\varepsilon 1} P_k - C_{\varepsilon 2} f_{\varepsilon 2}\tilde{\varepsilon}) + E + Y_c \tag{17}$$

where E, Y_c, $f_{\varepsilon 1}$, and $f_{\varepsilon 2}$ are the correction terms, which are given by

$$E = 2\nu\nu_t\left(\frac{\partial^2 U_i}{\partial x_j \partial x_k}\right)^2 \tag{18}$$

$$Y_c = \mathrm{Max}\left[0.83\left(\frac{k^{\frac{3}{2}}}{C_l\tilde{\varepsilon}y} - 1\right)\left(\frac{k^{\frac{3}{2}}}{C_l\tilde{\varepsilon}y}\right)^2\frac{\tilde{\varepsilon}^2}{k}, 0\right] \tag{19}$$

$$f_{\varepsilon 1} = 1 \tag{20}$$

$$f_{\varepsilon 2} = 1 - 0.3\exp\left(-R_t^2\right) \tag{21}$$

where C_l is 2.5. The additional source term in the dissipation equation (17) Y_c was originally introduced by Rhie and Chow,[13] whose role is to prevent the near-wall length scale from becoming too large in a recirculating flow region. Computations in this study showed that the correction factor Y_c in the L–S model is needed in order to maintain the stability of the computational process.

Modeling of Whisper Cages

Across the whisper-cage plate the governing momentum and energy equations are simulated as a porous-media model and can be written as follows:

Momentum equation:

$$0 = \frac{\mathrm{d}\langle P\rangle}{\mathrm{d}x} - \frac{\mu_{\mathrm{eff}}}{K}\langle U\rangle^2 + \frac{\mu_{\mathrm{eff}}}{\beta}\frac{\mathrm{d}^2\langle U\rangle}{\mathrm{d}y^2} \tag{22}$$

Energy equation:

$$\rho c_p\langle U\rangle\frac{\partial\langle T\rangle}{\partial x} = \frac{\partial}{\partial y}\left(\lambda\frac{\partial\langle T\rangle}{\partial y} - \beta\langle\gamma_U\gamma_T\rangle\right) \tag{23}$$

Transformation of Governing Equations

The transport equations used in the study were transformed into a three-dimensional curvilinear coordinate system.

The flow pass configuration was created by employing a grid-generation technique based on the two-dimensional internal flow grid generation.[9] This method is particularly advantageous for computations of a flow, which is bounded by solid boundaries.

For general three-dimensional configurations it is usually very difficult to obtain a reasonable grid with the entire physical region transformed into a single rectangular block. The technique used in this study follows the path of Thompson.[5] In this approach complete continuity can be achieved at the subregion interfaces by noting the correspondence of points exterior to one subregion with points interior to another. The necessary bookkeeping can be accomplished, and the coding complexity can be greatly reduced, by using an auxiliary layer of points just outside each of the six sides of the computational region, analogous to the procedure for two dimensions. A correspondence is then established in the code between the auxiliary points and the appropriate points just inside other subregions.

General three-dimensional regions were built up using subregions. First, point distributions are specified on the edges of a curved

surface forming one boundary of a subregion, and a two-dimensional coordinate system was generated on the surface. When this has been done for all surfaces bounding the subregion, the three-dimensional system within the subregion is generated using the points on the surface grids as boundary conditions. All of these steps were performed interactively so that the user is able to monitor the generation and alter the grid by varying parameters. Equations (2), (6), (7), and (18) can be written in the following general form:

$$\text{div}[\rho\bar{U}\phi - G_\phi \text{grad}(\phi)] = S_\phi \tag{24}$$

where ϕ is an arbitrary transport variable and $\bar{U}$ is the velocity vector. Equation (24) is transformed from the polar cylindrical coordinates (r, θ, z) into generalized curvilinear coordinates. In the new coordinate system Eq. (24) becomes

$$\frac{1}{J}\left[\frac{\partial(\rho\tilde{U}\phi)}{\partial\xi} + \frac{\partial(\rho\tilde{V}\phi)}{\partial\eta} + \frac{\partial(\rho\tilde{W}\phi)}{\partial\zeta}\right] = \frac{1}{J}\frac{\partial}{\partial\xi}\left[\frac{G_\phi}{J}(j_{11}\phi_\xi + j_{21}\phi_\eta + j_{31}\phi_\eta)\right] + \frac{1}{J}\frac{\partial}{\partial\eta}\left[\frac{G_\phi}{J}(j_{12}\phi_\xi + j_{22}\phi_\eta + j_{32}\phi_\eta)\right] + \frac{1}{J}\frac{\partial}{\partial\zeta}\left[\frac{G_\phi}{J}(j_{13}\phi_\xi + j_{23}\phi_\eta + j_{33}\phi_\eta)\right] + S(\xi, \eta, \zeta) \tag{25}$$

where $\tilde{U}$, $\tilde{V}$, $\tilde{W}$ are contravariant velocities. These are given as

$$\tilde{U}_i = e_{ji}U_j \tag{26}$$

where

$$e_{ij} = q_{ij}^2 \tag{27}$$

and where

$$q_{ij} = \varepsilon_{ijk}\frac{\partial}{\partial\xi_i}x_k \tag{28}$$

Also G_ϕ represents the diffusion coefficient.

Numerical Method

The system of the equations is solved by using the nonstaggered finite volume difference (FVD) method. Compared with the staggered FVD method, the nonstaggered FVD has several advantages: it is easier to program, and it requires less CPU time. However, it is well known that oscillation of pressure and velocity can appear with nonstaggered FVD. Fortunately, Rhie and Chow[13] successfully solved these oscillatory problems by using the interpolation method, where the flux flowing through a control volume surface is linked with the pressures at the neighboring nodes. Keeping these observations in mind, a brief summary of the numerical model used in this study is provided here:

1) Grids were generated by using the algebraic grid-generation technique developed by Maruszewski and Amano.[9]

2) The computational domain is discretized, and both scalar and vector variables are located at the common grid position as opposed to staggered grid arrangements. Here, the method of Rhie and Chow[13] is adopted for the nonstaggered grid formulations.

3) The linkage between the continuity and momentum equations is carried out through the SIMPLEC method by Van Doormaal and Raithby.[14]

4) The convection–diffusion string was handled by using the QUICK scheme of Leonard.[15]

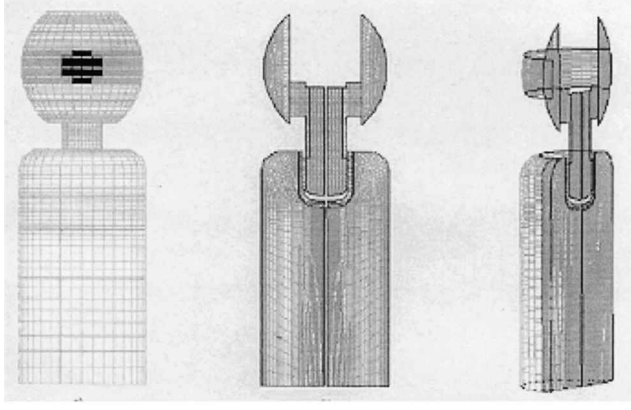

Fig. 2 Three different views of the grid: a) surface grid, b) inside view, and c) three-dimensional view.

Table 1 Inlet Conditions

Property	100% open	85% open	50% open
Inlet pressure, Pa	1.24E+7	1.24E+7	1.24E+7
Outlet pressure, Pa	9.12E+5	7.09E+5	4.26E+5
Inlet temperature, K	799	799	799

Table 2 Physical properties

Viscosity	2.8E−5 kg/m s
Thermal conductivity	0.1 W/kg K
Specific heat	2500 J/kg K

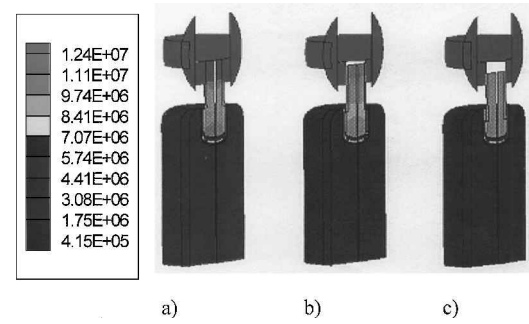

Fig. 3 Absolute static pressure (Pa) for a) 100% open, b) 85% open, and c) 50% open.

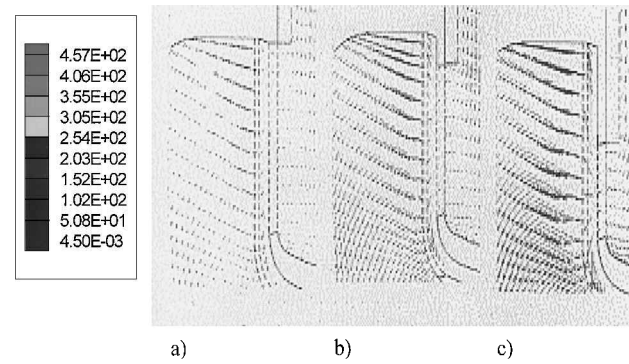

Fig. 4 Velocity vectors (m/s) at the entrance to the bypass pipe for a) 100% open, b) 85% open, and c) 50% open.

3) The linkage between the continuity and momentum equations is carried out through the SIMPLEC method by Van Doormaal and Raithby.[14]

4) The convection–diffusion string was handled by using the QUICK scheme of Leonard.[15]

Three different views of the grid structure are also depicted in Fig. 2 for the 85%-open case. The grid for the 100% and 50%-open cases has the same number of cells in it. Prior to the selection of the grid system, numerous grid-independent tests were performed in the range 50,000 and 120,000. It was discovered that the grid with 120,000 still can be handled in the Power Challenge Array—one of the supercomputers at National Center for Supercomputing Applications (NCSA). After these tests it was concluded that the grid with $47 \times 20 \times 81$ (a total of 76,140 cells) is appropriate for the case of 100% valve opening by showing only 1–2% variations in the mean-flow variables including the pressure, velocities, and temperature when the number of grids varies from 70,000 to 120,000. However, the grid for the 85%-open case had to be enlarged slightly in order to accommodate the extra 5% opening. The total number of cells in the 85%-open grid is 78,020. It is a $47 \times 20 \times 83$ grid. The grid spacing is a little finer in the region where the steam exits the bypass valve and enters into the pipe. This permits better results in a location where significant changes in the

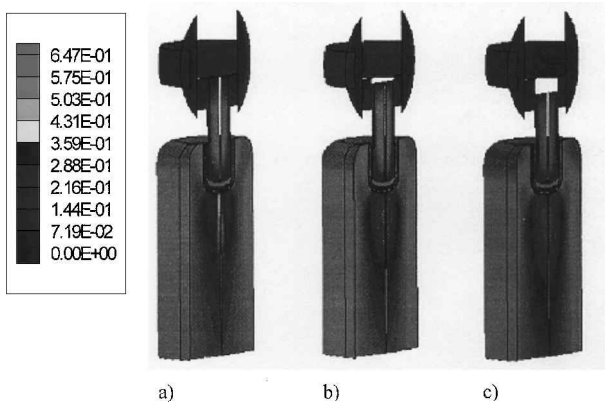

Fig. 5 Mach number for a) 100% open, b) 85% open, and c) 50% open.

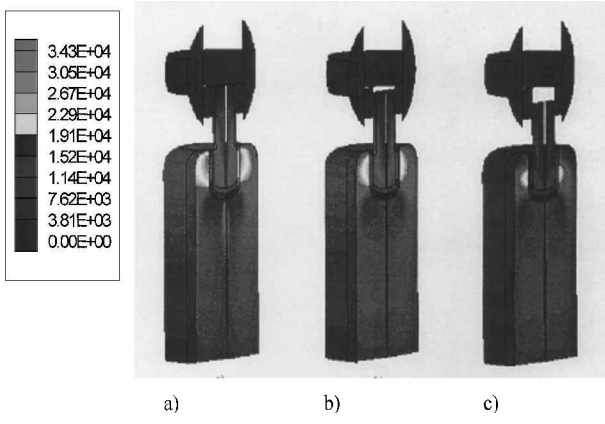

Fig. 6 Turbulent kinetic energy (m^2/s^2) for a) 100% open, b) 85% open, and c) 50% open.

flow occur. The computed y^+ for the first grid line from the wall varied from 5 to 30.

The inlet conditions for the steam used for the computations of three different valve opening cases are listed in Table 1. These values were recalculated based on the temperature at each node by employing the empirical property correlations, which are the function of the temperature. The physical constants specified for the steam are given in Table 2. Density is calculated through the ideal-gas law.

Presentation of Results

Figure 3 shows the large pressure drop that occurs through the valve. The largest drop in the pressure occurs through the two lower whisper cages. It is here that the highest resistance to the flow does occur downstream of the valve; the pressure remains relatively constant because the only loss the flow experiences is caused by friction.

The velocity vectors across the whisper cage are shown in Fig. 4. Inside the bypass valve the steam flows show a very low velocity except near the center of the valve. This is caused by the high pressure in the valve. However, as the flow passes out of the bypass valve through the whisper cage, it accelerates because it encounters a low-pressure region. In the areas where recirculation occurs, the velocity magnitude is also small. Recirculation occurs as a result of the steam exiting the valve normal to the centerline of the pipe. The steam is at its highest velocity as it exits the bottom of the bypass valve through the "draining hole" created at the bottom of the valve. Again this is caused by the flow encountering a low-pressure region.

The flow moves slowly inside the bypass valve. As a result, the velocity vectors inside the valve are relatively constant and at a small magnitude. This can be seen in Fig. 4. Some acceleration of the velocity vectors occurs when the flow enters into the vertical section of the valve and travels toward the valve exit.

For the most part the entire flow is subsonic. This can be seen from Fig. 5, which shows the Mach number of the flow. The only places where the flow becomes a high Mach number are at the middle of the valve and just downstream of the hole. At both locations the Mach

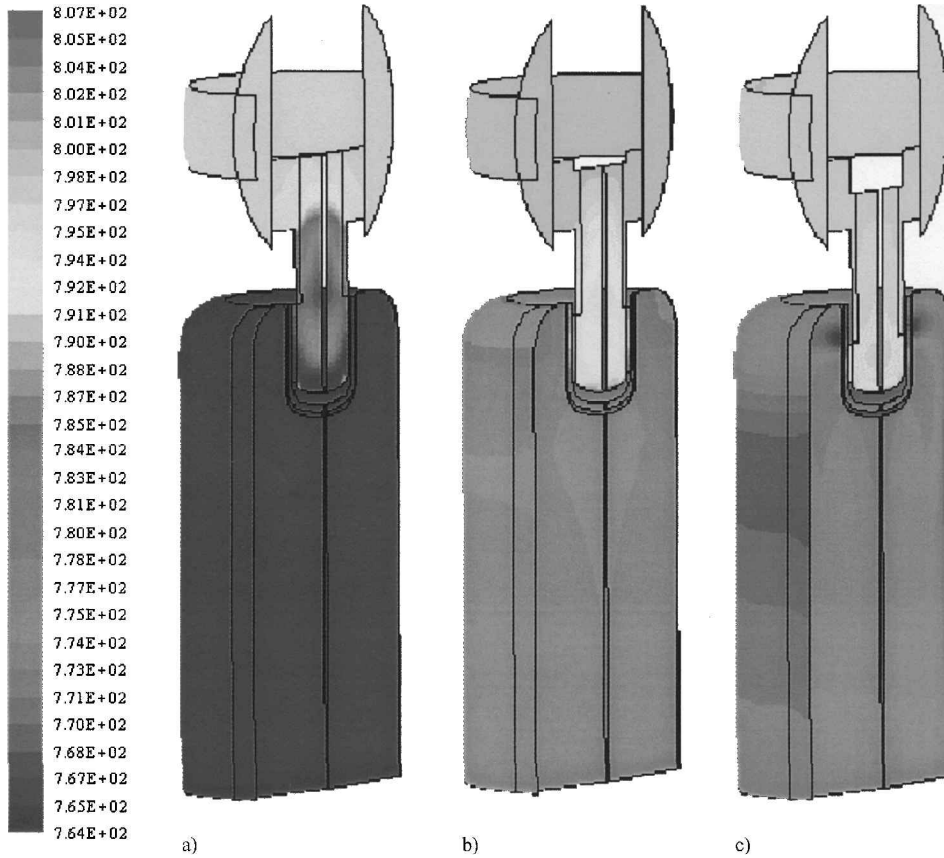

Fig. 7 Temperature (K) for a) 100% open, b) 85% open, and c) 50% open.

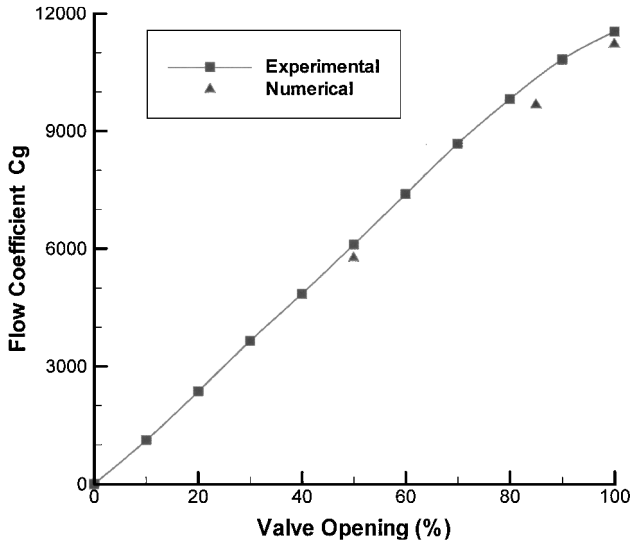

Fig. 8 Valve opening (%).

number exceeds 0.3. The Mach-number contours are very similar to the velocity magnitude contours and display the same results.

The highest turbulent kinetic energy (TKE) occurs where the flow leaves the bypass valve and enters into the pipe. This is shown in Fig. 6. As the steam exits the valve, entering the relatively low-pressure region in the pipe, it experiences highly skewed shear action, which causes the TKE to enhance significantly. The TKE gradually decreases downstream from the valve as a result of the flow becoming more stable downstream. Also, wherever there is recirculation the TKE becomes low.

The temperature distributions are shown in Fig. 7 for three valve opening cases. The highest temperature occurs at the inlet region when the valve is fully open. However the location of the peak temperature moves to the valve throat for 85% open and 50% open. As the steam goes through the core of the valve, it experiences highly skewed velocity, which causes the temperature to become high in the throat for both 85 and 50% openings. The temperature gradually decreases toward the exit of the valve.

The gas-sizing coefficient is one of the indicators for the flow rate estimates through the valve. This defined to relate critical flow to the absolute pressure as follows:

$$Q_{\text{conventional}} = C_g P_{\text{in}} \tag{29}$$

The flow characteristic curve can be seen in Fig. 8. It is a plot of the gas-sizing coefficient C_g vs the percentage of the valve opening. The value of C_g was calculated for the three opening cases using the Universal Gas Sizing Equation. These three values were plotted along with the experimental data provided by Fisher.[16] It can be seen that numerical data obtained in this analysis produced C_g values that agree with the experimental values within 15% error.

Conclusions

The task of modeling and computing flow behaviors in the high-pressure turbine bypass valve has been successfully accomplished for three different opening cases. Several conclusions emerged throughout this study, which are summarized as follows:

1) The largest drop in pressure occurs through the lowest whisper cage. It is here that the highest resistance to the flow occurs. Downstream of the valve the pressure remains relatively constant because the only losses the flow incurs are caused by friction between the wall and the flow.

2) The highest turbulent kinetic energy occurs where the flow leaves the bypass valve and enters into the pipe. As the steam exits the valve and enters the relatively low-pressure region in the pipe, it experiences an acceleration, which causes the TKE to increase. The TKE gradually decreases downstream from the valve because of the flow becoming more stable downstream. Also, wherever there is recirculation the TKE is small.

3) It was shown that numerical data obtained in this analysis produced C_g values that agree with the experimental values.

4) Finally, it can be emphasized that the numerical model developed in this study successfully predicts flows and heat transfers in a complex valve geometry with huge pressure-drop flows. This model can be used for design improvements of such turbine bypass flow systems.

Acknowledgments

This project is currently supported by Moritani Corporation. Thanks go to Nippon Fisher Co., Ltd., which provided numerous data and suggestions. The authors are grateful to National Science Foundation (NSF) because all of the computations were made on the supercomputer (Power Challenge Array) under Grant NSF CTS 970045N.

References

[1]Launder, B. E., Reece, G. J., and Rodi, W., "Progress in the Development of a Reynolds-Stress Turbulence Closure," *Journal of Fluid Mechanics*, Vol. 68, Pt. 3, 1975, pp. 537–566.

[2]Amano, R. S., Goel, P., and Chai, J. C., "Turbulence Energy and Diffusion Transport of Third-Moments in a Separating and Re-Attaching Flow," *AIAA Journal*, Vol. 26, No. 3, 1988, pp. 273–282.

[3]Amano, R. S., and Chai, J. C., "Transport Models of the Turbulent Velocity-Temperature Products for Computations of Recirculating Flows," *Numerical Heat Transfer*, Vol. 14, No. 1, 1988, pp. 75–95.

[4]Chai, J. C., and Amano, R. S., "Application of Higher-Order Turbulence Closure Model to Plane Jet," *Numerical Heat Transfer*, Vol. 21, Pt. A, 1992, pp. 21–35.

[5]Thompson, J. F., "Numerical Solution of Flow Problems Using Body-Fitted Coordinate Systems," *Computational Fluid Mechanics*, edited by W. Kollmann, Hemisphere, NY, 1980, pp. 1–98.

[6]Shyy, W., Tong, S. S., and Corea, S. M., "Numerical Recirculating Flow Calculation Using a Body-Fitted Coordinate System," *Numerical Heat Transfer*, Vol. 8, 1985, pp. 99–113.

[7]Peric, M., "Efficient Semi-Implicit Solving Algorithm for Nine-Diagonal Coefficient Matrix," *Numerical Heat Transfer*, Vol. 11, 1987, pp. 251–279.

[8]Hutchinson, B. R., Galpin, P. F., and Raithby, G. D., "Application of Additive Correction Multi-Grid to the Coupled Fluid Flow Equations," *Numerical Heat Transfer*, Vol. 13, 1987, pp. 133–147.

[9]Maruszewski, J. P., and Amano, R. S., "Grid Generation and Its Application to Separated Flows," *Numerical Heat Transfer, Part B*, Vol. 21, 1992, pp. 183–197.

[10]Amano, R. S., and He, T., "Calculation of Stator-to-Rotor Flow-Field by Using a Second-Order Turbulence Closure," *Proceedings of the Ninth Symposium on Turbulent Shear Flows*, Springer-Verlag, NY, Vol. 3, No. 30-3, 1993, pp. 30.3.1–30.3.6.

[11]Iacovides, H., and Launder, B. E., "Parametric and Numerical Study of Fully-Developed Flow and Eat Transfer in Rotating Duct," *Journal of Turbomachinery*, Vol. 113, 1987, pp. 331–338.

[12]Launder, B. E., and Sharma, B. I., "Application of the Energy Dissipation Model of Turbulence to Flow Near a Spinning Disc," *Letters in Heat Mass Transfer*, 1974, p. 2.

[13]Rhie, C. M., and Chow, W. L., "Numerical Study of the Turbulent Flow Past an Airfoil with Trailing Edge Separation," *AIAA Journal*, Vol. 21, No. 11, 1983, pp. 1525–1532.

[14]Van Doormaal, J. P., and Raithby, G. D., "Enhancements of the SIMPLE Method for Predicting Incompressible Fluid Flows," *Numerical Heat Transfer*, Vol. 7, 1984, pp. 147–163.

[15]Leonard, B. P., "A Stable and Accurate Convective Modelling Procedure Based On Quadratic Upstream Interpolation," *Computational Methods for Applied Mechanical Engineering*, Vol. 19, 1979, pp. 59–98.

[16]Fisher, "Bulletin 85.2," *Computational Methods for Applied Mechanical Engineering*, Fisher-Rosemount Company, 1997.